Microchimica Acta (2020) 187:230
https://doi.org/10.1007/s00604-020-4188-9

ORIGINAL PAPER

An optical biosensor for the determination of cathepsin B as a cancer-associated enzyme using nanoporous anodic alumina modified with human serum albumin-thionine

Mahmoud Amouzadeh Tabrizi[1] · Josep Ferré-Borrull[1] · Lluis F. Marsal[1]

Received: 9 September 2019 / Accepted: 24 February 2020

Abstract

An interferometric reflectance spectroscopy-based biosensor for the determination of cathepsin B (Cat B) as a cancer-related enzyme has been fabricated. For this purpose, the nanoporous anodic alumina (NAA) was fabricated electrochemically. The NAA was then modified with the amino-silane coupling agent. After that, human serum albumin (HSA) was immobilized into the NAA pores by using glutaraldehyde as a cross-linking agent. Subsequently, the carboxylic group of HSA was activated with N-ethyl-N′-(3-(dimethylamino)propyl)carbodiimide (EDC) and N-hydroxysuccinimide (NHS) to attach to thionine (TH) as a photoprobe to fabricate the labeled HSA (HSA-TH). HSA-TH plays a significant role in this sensor to determine cathepsin B as a model analyte for the development of the interferometric reflectance spectroscopy-based biosensor for the measurement of protease. The attached TH adsorbed the illuminated white light on NAA modified with HSA-TH. Therefore, the intensity of the reflected light to the charge-coupled device (CCD) detector decreased in the wavelength range 450–1050 nm. In the presence of Cat B, HAS-TH cleaved into short peptide fragments and washed away by flow cell system. Since TH was removed from NAA, the intensity of the reflected light increased. The peak area has a logarithmic relationship with the concentration of Cat B in the range 0.5 to 64.0 nM. The limit of detection of the biosensor sensor was 0.08 nM. The optical sensor was used for the determination of Cat B in a human serum sample.

Keywords Interferometric reflectance spectroscopy · Biosensor · Nanoporous anodic alumina · Cathepsin B

Introduction

Cathepsin B (Cat B) is an important biomarker in the identification of many cancer types such as lung cancer, colorectal cancer, breast cancer, oral cancer, brain cancer, liver cancer, and prostate cancer [1, 2]. Therefore, it is important to develop a reliable biosensor for the detection of Cat B. Various techniques have been reported for Cat B sensing such as electrochemical [2, 3], fluorescence [4], surface plasmon resonance [5]. However, these methods are expensive, critical operational conditions.

Interferometric biosensors based on porous materials are a type of optical biosensors can be used for sensing biomolecules [6–8]. In these sensors, a light beam is illuminated on the porous material films such as nanoporous anodic aluminum (NAA) [9, 10], microporous silicon [11], nanoporous titanium [12], and then reflected into a charge-coupled device (CCD) detector. A light beam is reflected on top of the porous material film (interface I), and part of the light travels through the pores, where bio-receptors (such as aptamer, antibody), are immobilized on the inner wall of the pores, until it is reflected at the bottom of the pores (interface II). The superposition of these two reflected light waves generates a series of constructive and destructive interferences. The position of these waves' interferometric fringes is governed by the Fabry-Perot relation. When the reflected light at the interface I and the interface II overlap at a CCD detector, a spectrum with a lot of fringes (Fabry-Perot fringe spectrum) will be recorded

Electronic supplementary material The online version of this article (https://doi.org/10.1007/s00604-020-4188-9) contains supplementary material, which is available to authorized users.

✉ Lluis F. Marsal
lluis.marsal@urv.cat

[1] Departamento de Ingeniería Electrónica, Eléctrica y Automática, Universitat Rovira i Virgili, Avda. Països Catalans 26, 43007 Tarragona, Spain

Published online: 13 March 2020

because of their optical path difference. After the interaction of the immobilized bio-receptors on the pores of the substrate, the optical property (intensity and wavelength) of the reflected light at the interface II will be changed. This change leads to a change in the Fabry-Perot fringe spectrum [6].

Among the various porous material films, the NAA film is more interested in the fabrication of optical biosensors, because of its low cost, high biocompatibility, good functionalization capacity with silane coupling agents to immobilization of biomolecules, high stability, high surface area, easy fabrication, and good optical property [13, 14].

Interferometric biosensors are cheap, easy operation conditions, and remote sensing of targets. However, the sensitivity of this kind of sensor is low. Therefore, finding a solution for this problem is a big challenge for researchers. According to the previous reports, the intensity of the reflected light from NAA-based biosensor into the CCD detector could be changed during the desorption [6] or absorption [15] of the photoprobe molecule that has a high adsorption coefficient (such as methylene blue). Therefore, this strategy can be applied for the determination of the proteases as biomarkers. Cat B is a lysosomal cysteine protease that cleaves the peptides to small

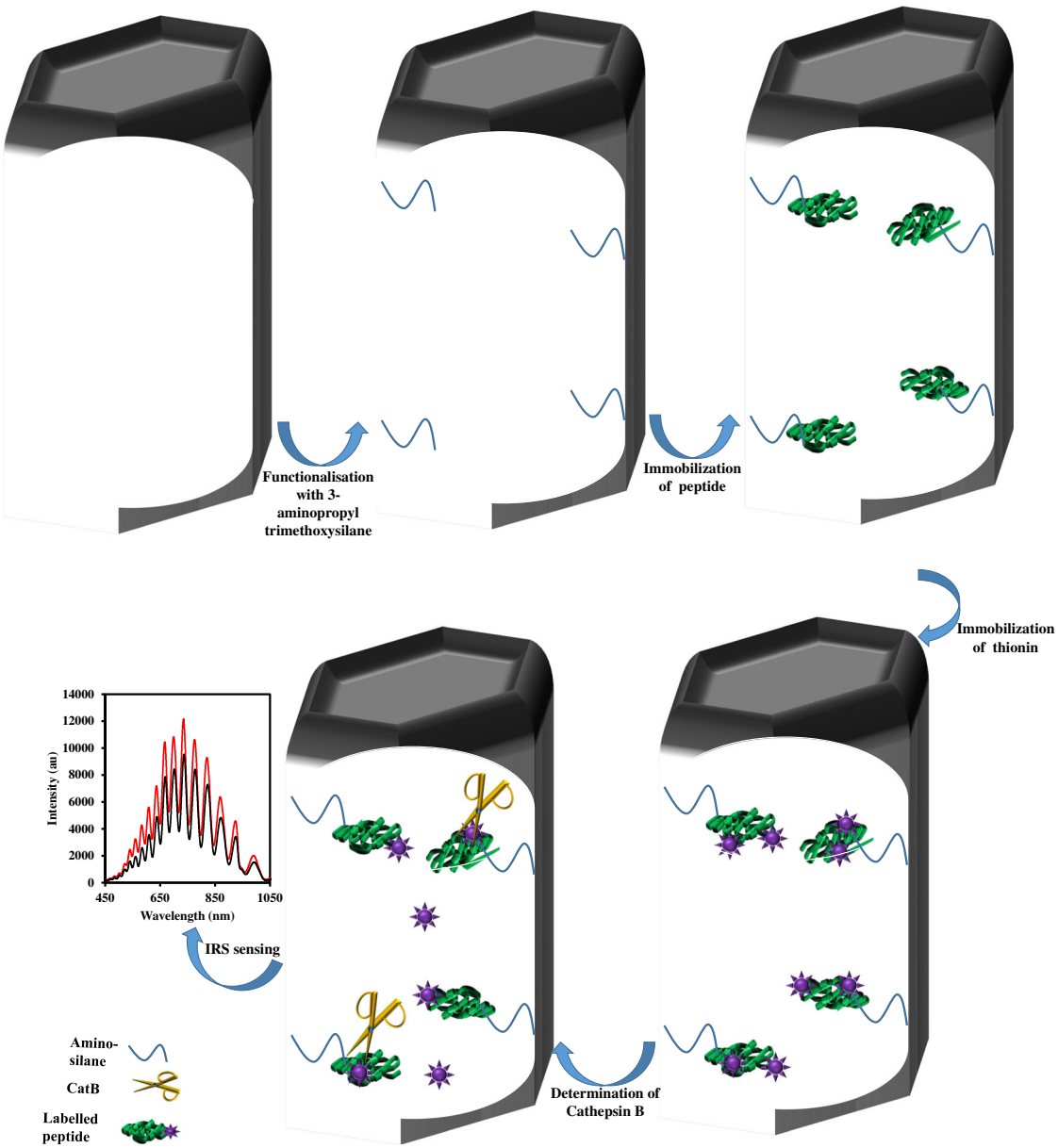

Fig. 1 The schematic illustration for the fabrication of NAA-Gla-HSA-TH

fragments from the carboxyl side of arginine, leucine, glycine, and lysine residues selectively [16].

Thionine (TH) that is structurally related to methylene blue can be a good candidate for the fabrication of the labeled peptide because of two reasons: first, it has two primary amine groups that can interact with the activated carboxylic group of the peptide such as HSA. Second, the absorption coefficient of it is so high (5.85×10^4 dm^3 mol^{-1} cm^{-1}) [17].

Therefore, the labeled peptide can be used for the determination of Cat B by using the interferometric biosensors.

To the best of our knowledge, there have been no reports about the interferometric biosensors to determine Cat B, yet. In this study, human serum albumin labeled with thionine (HSA-TH) has been immobilized on the pore wall of NAA. The results showed that the intensity of the reflected light to the CCD detector in the presence of Cat B changed, severely. This change in the intensity of the reflected light has a good linear relationship with the logarithm of Cat B. On the basis of these great advantages, the biosensor showed high analytical performance in terms of sensitivity, selectivity, stability, linear dynamic range (LDR), and limit of detection (LOD).

Experimental section

Reagents and chemicals

All chemicals were of analytical reagent grade and used without further purification. The details are denoted in the electronic supporting material.

Apparatus

The interferometric reflectance spectra were obtained using an AvaSpec-ULS3648 fiber optic spectrometer. Scanning electron microscopy (SEM) was obtained by using an FEI Quanta 600. Ultraviolet-visible (UV-Vis) absorption spectrum was recorded using a PerkinElmer UV-Vis spectrophotometer. Infrared spectra were obtained by using a JASCO FT/IR-680 Plus Fourier transform infrared (FTIR) spectrometer. Raman spectra were obtained using a Renishaw's inVia Raman spectrometer using He–Ne lasers at $\lambda = 633$ nm with. EMItech K575X sputter coater was used to deposit 10-nm-thick gold layer under vacuum at 30 mA for 1 min.

The fabrication of the NAA-Gla-HSA-TH

The NAA was prepared based on the previous method [7, 18, 19]. The key steps of the fabrication of NAA include the following: Step 1: Electropolishing of Al in an ethanol solution containing perchloric acid (25%) under stirring condition by applying 20 V for 10 min at 5 °C. Step 2: Anodizing of the electropolished Al in oxalic acid solution under stirring condition by applying 40 V for 20 h at 5 °C. Step 3: Chemical etching of the anodized sample in 0.4 M phosphoric acid solution containing chromic acid (0.2 M) for 3 h at 70 °C. Step 4: Anodizing of the sample in oxalic acid solution under the same conditions as in Step 2, and it was done until a total charge of 20 C for each sample. Step 5: Pore widening by immersing of NAA in 5% phosphoric acid for 20 min under stirring condition.

The NAA was then rinsed with water for 30 s and dried under nitrogen gas flow. The NAA was then put

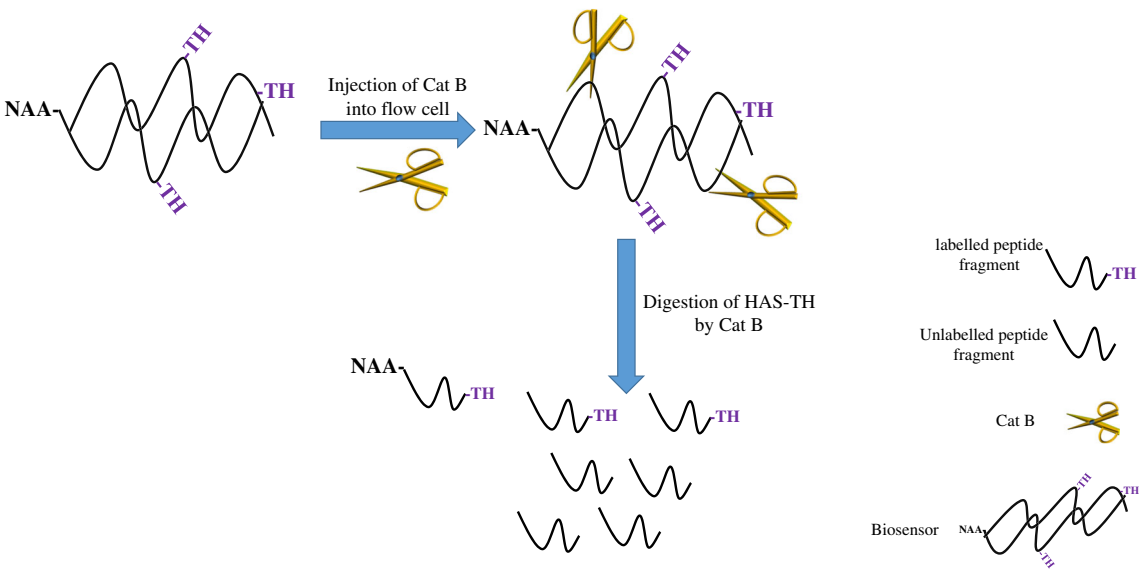

Fig. 2 The schematic illustration for the sensing mechanisms of Cat B

into ethanol/water solution (3:1) containing 1% (3-Aminopropyl)tiethoxysilane solution and kept under stirring and nitrogen gas atmosphere conditions for 30 min to functionalize the inner surface of the NAA nanopore with the amino group. After that, amino-functionalized NAA (NAA-NH_2) was rinsed with ethanol/water solution (3:1) for 1 min and dried under nitrogen gas flow. NAA-NH_2 was then dried under a nitrogen atmosphere at 100 °C for 2 h. Subsequently, NAA-NH_2 was immersed in glutaraldehyde (Gla) solution (2.5%) and stirred for 1 h at room temperature. The NAA-Gla was then washed with ethanol/water solution (3:1) and then dried with nitrogen gas flow. The NAA-Gla was then immersed in HSA solution (10 mL, 5 mM, 0.1 M PB, pH 7.4) and kept under the stirring condition for 12 h at room temperature. During this time, the amino-terminal groups of HSA were attached to the aldehyde groups of Gla, immobilizing on NAA. After that, the NAA-Gla-HSA was rinsed thoroughly with double-distilled water to wash away the loosely adsorbed HSA. After that, the NAA-Gla-HSA was immersed in the solution PB solution containing 40-mM EDC and 90-mM NHS for 5 h to activate the carboxylic groups of HSA to interact with primary amine groups of TH. The NAA-Gla-HSA was then washed quickly with deionized water and immersed in a TH solution (50 mM) for 12 h. Finally, the NAA-Gla-HSA-TH washed with dual deionized water to wash away loosely adsorbed TH.

The schematic representation for the fabrication of the NAA-Gla-HSA-TH and the sensing mechanism is shown in Fig. 1.

The sensing process of Cat B

For this purpose, different concentration of Cat B was transferred into the measuring cell by using a peristaltic pump. Cat B is a protease that can cleave off the proteins such as HSA at pH 5 solution from the carboxyl-terminal side of arginine and lysine to short peptide fragments [16]. Therefore, when Cat B solution was pumped to the measuring cell, it started cleaving HSA-TH to short peptide fragments. During this process, the optical properties of NAA-Gla-HSA-TH changed significantly. The change in the optical properties included a blue shift in wavelength and an increase in the intensity of the reflected light to the detector. The reasonable explanation is that the cleavage of HSA-TH from NAA-Gla-HSA-TH decreased the amount of attached peptide-TH. The decrease in the amount of attached TH that could adsorb white light led to an increase in the intensity of the reflected light to the CCD detector. The increase in the intensity of the reflected light consequent on the increase in the peak area.

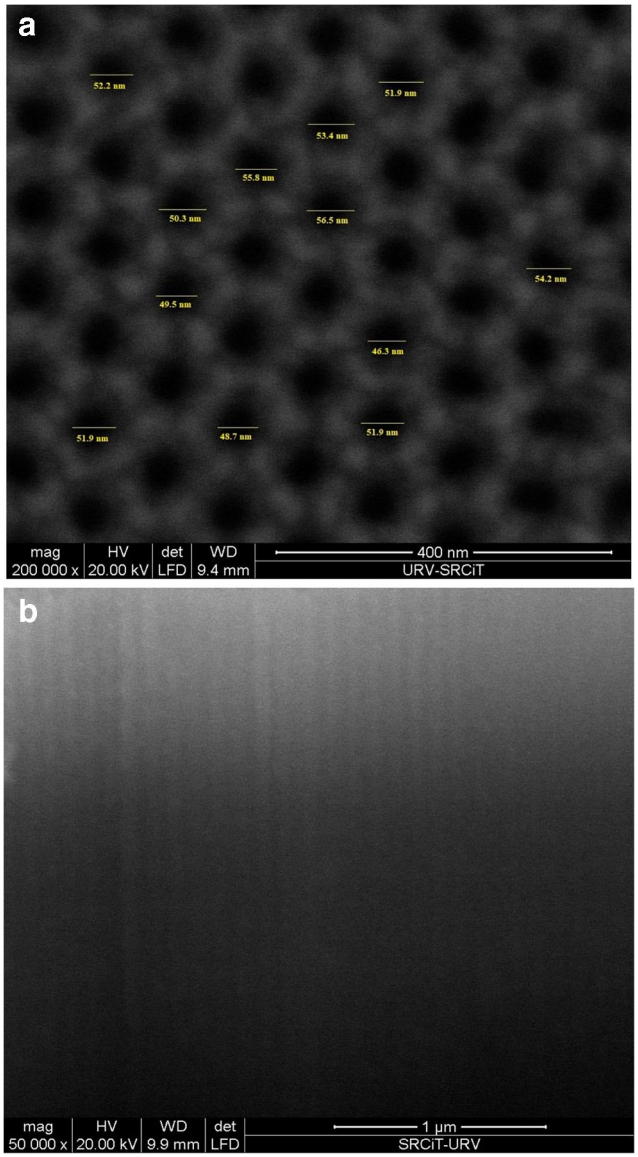

Fig. 3 SEM images of NAA: (**a**) top view and (**b**) cross-section view

On the other hand, the cleavage of the peptide bonds in HSA from the carboxyl side of arginine and lysine that is considered as a desorption process caused a blue shift in the wavelength of the reflected light.

Figure 2 shows the schematic diagram of the sensing process of Cat B by using NAA-Gla-HSA-TH.

Results and discussion

The surface morphology of the NAA

The morphological characterization of the NAA was studied by SEM (Fig. 3). Top view (a) and (b) cross-section view of NAA show that this nano-platform has a three-dimensional hexagonal multi-pore structure. The average diameter pore

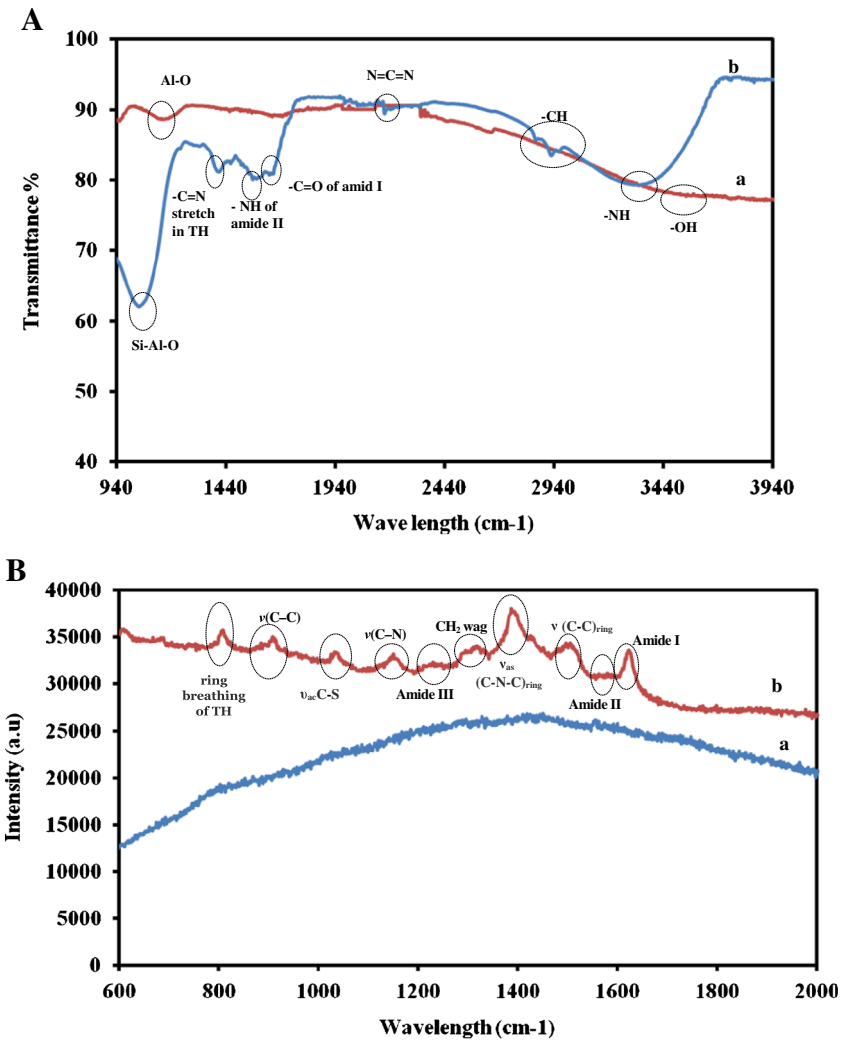

Fig. 4 **A** FTIR, **B** Raman spectra of NAA (*a*) and NAA-Gla-HSA-TH (*b*)

size of NAA was estimated to be 50 ± 2 nm. This three-dimensional structure of the NAA provides a high surface area for the immobilization of biomaterials.

Characterization of NAA-Gla-HSA-TH

FTIR (A) and Raman (B) spectroscopy were employed to characterize the structure of NAA and NAA-Gla-HSA-TH (Fig. 4). Figure 4A (curve a) shows the FTIR spectrum recorded for NAA in which an absorption band at 3440 cm^{-1} due to the –OH stretching and a band at 1153 cm^{-1} due to the –Al-O stretching are clearly seen [20].

However, after the immobilization of HSA-TH into the NAA nanopore, several new absorption bands appeared. As shown in Fig. 4A (curve b), an absorption band at 3310 cm-1 due to the –NH stretching at 2963 cm-1, 2928 cm-1 and 2898 due to the –CHx stretching, a weak band at 2353 cm-1 due to the –C=NH+, a weak band at 2161 cm-1 due to the –N=C=N stretching, a band at 2161 cm-1 due to the –C=O stretching of amide I, a band at 1575 cm-1 due to the –N-H stretching of amide II, and a band at 1405 cm-1 due to the –C=N stretching of TH and a band at 1037 cm-1 due to the –Si-Al-O stretching [21–24] are seen clearly.

NAA (curve a) and NAA-Gla-HSA-TH (curve b) were also characterized by Raman spectroscopy (Fig. 4B). As can be seen in Fig. 4B (curve a), Raman spectrum of NAA had not any strong band in the wavelength range of 600–2000 cm^{-1}. However, after the immobilization of HSA-TH into the NAA, Raman spectrum of the sample changed significantly (Fig. 4B, curve b). As shown in this figure, a band at 1625 cm^{-1} due to –C=C (amide I), a band at 1582 cm^{-1} due to the –CN (amide II) of HSA, a band at 1507 cm^{-1} due to the –C-C stretching vibrations in aromatic rings of TH, a band at 1382 cm^{-1} due to the –C-N-C of TH, a band at 1323 cm^{-1} due to the $–CH_2$

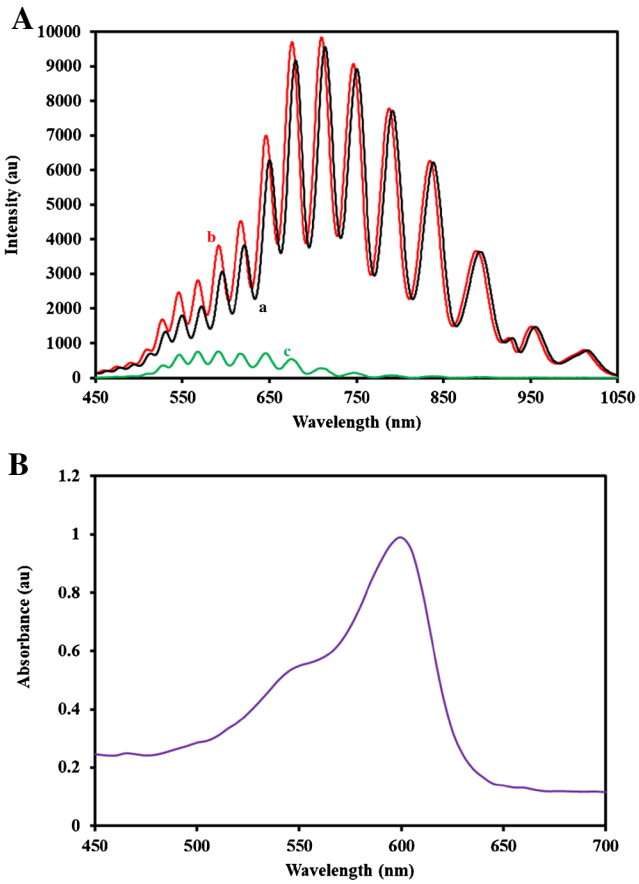

Fig. 5 **A** Fabry-Perot fringe spectrum of NAA-Gla-HSA-TH before (*a*) and after (*b*) interaction with 64 nM of Cat B and (*c*) the difference between the interference spectra of (*a*) and (*b*) in acetate buffer (0.1 M, pH 5.0). **B** UV-Vis absorption spectra of TH solution in acetate buffer (0.1 M, pH 5.0)

wag of HSA, a band at 1235 cm^{-1} due to amide III of HSA, a band at 1158 cm^{-1} due to the –C-N of HSA a band at 1036 cm^{-1} due to the –C-S of TH, a band at 909 cm^{-1} due to the –C-C of HSA, and a band at 808 cm^{-1} due to ring breathing of TH are seen [25, 26]. The results of FTIR and Raman spectra prove the immobilization of HSA-TH into the NAA.

The optical characterization of the NAA-Gla-HSA-TH

Figure 5a shows the Fabry-Perot fringe spectrum of the NAA-Gla-HSA-TH before (curve a) and after (curve b) injection of Cat B solution (64 nM, 0.1 M acetate buffer, pH 5.0) in the wavelength range of 450–1050 nm. As can be seen, the intensity of the spectrum of NAA-Gla-HSA-TH in the range of 500–700 nm increased after interaction with Cat B. On the other hand, UV-Vis absorption spectroscopy of TH solution showed that TH adsorbed the light in the range 510–640 nm (Fig. 5b). The reasonable explanation is that Cat B cleaved the HSA-TH to small peptide fragments (TH-peptide and unlabeled peptide) and then washed away by fellow cell system. Therefore, the amount of the immobilized TH on biosensor decreased, and consequently the intensity of the reflected light to the CCD detector increased.

In addition, as shown, the Fabry-Perot fringe spectrum shifted to low wavelength due to a decrease in the refractive index of biosensor during cleavage of HSA-TH into small peptide fragments that is considered as desorption process.

According to the previous report, both the change in the intensity [6] and the wavelength [7] of the reflected light can be used for the determination of targets. The change in the intensity of the reflected light caused a change in the peak area of the Fabry-Perot fringe spectrum in the wavelength range of 450–1050 nm and a change in the wavelength of the reflected light that caused a change in the effective optical thickness (EOT) of NAA-Gla-HSA-TH. According to the results obtained, the change in the peak area of the Fabry-Perot fringe spectrum (Δpeak area = 104,370.0 a.u) was 3727 times bigger than the amount of the change in the EOT (ΔEOT = 28.0 nm) of NAA-Gla-HSA-TH in the presence of 64.0 nM. Therefore, the change in the peak area as a signal was considered versus the concentration of Cat B throughout this research.

Optimization of effective parameters on the response of the NAA-Gla-HSA-TH

Figure S1 shows the effect of the pH of the solution (A) and time needed to digest of HSA by Cat B (16.0 nM) (B). As can be seen, the optimum pH of the solution is 5 that has a good agreement with the previous reports [2, 27]. According to these reports, the maximum activity of Cat B is at pH 5.0. Also, the response of the NAA-Gla-HSA-TH increased rapidly with increasing interaction time up to 45 min and remained unchanged at longer incubation times, indicating the digestion process of HSA-TH to small peptide fragment by Cat B has reached to the saturation level. Therefore, 45 min and solutions with a pH 5.0 have been applied as the optimum condition throughout this research. All parameters were optimized at 37 °C.

Determination of cat B

Figure 6 shows the obtained Fabry-Perot fringe spectrum of NAA-Gla-HSA-TH in the absence and presence of different amounts of Cat B. As shown in Fig. 6a, after digesting HSA-TH by Cat B, the intensity of the reflected light to the CCD detector increased. The calibration equation was linear in the concentration range of 0.5–64.0 nM (Fig. 6b) with a regression equation of $\Delta\text{peak area} = 3.7 \times 10^4 \text{ Log } C_{\text{Cat B}}\ (\text{nM}) + 3.9 \times 10^4$ ($R2 = 0.9893$, $n = 7$) (Fig. 6b). The limit of detection (LOD) was found to be 0.08 nM (at $3\sigma/S$), where σ is the standard deviation of the blank measurements and S is the slope. The LOD of the proposed sensor was lower than the previous report [3].

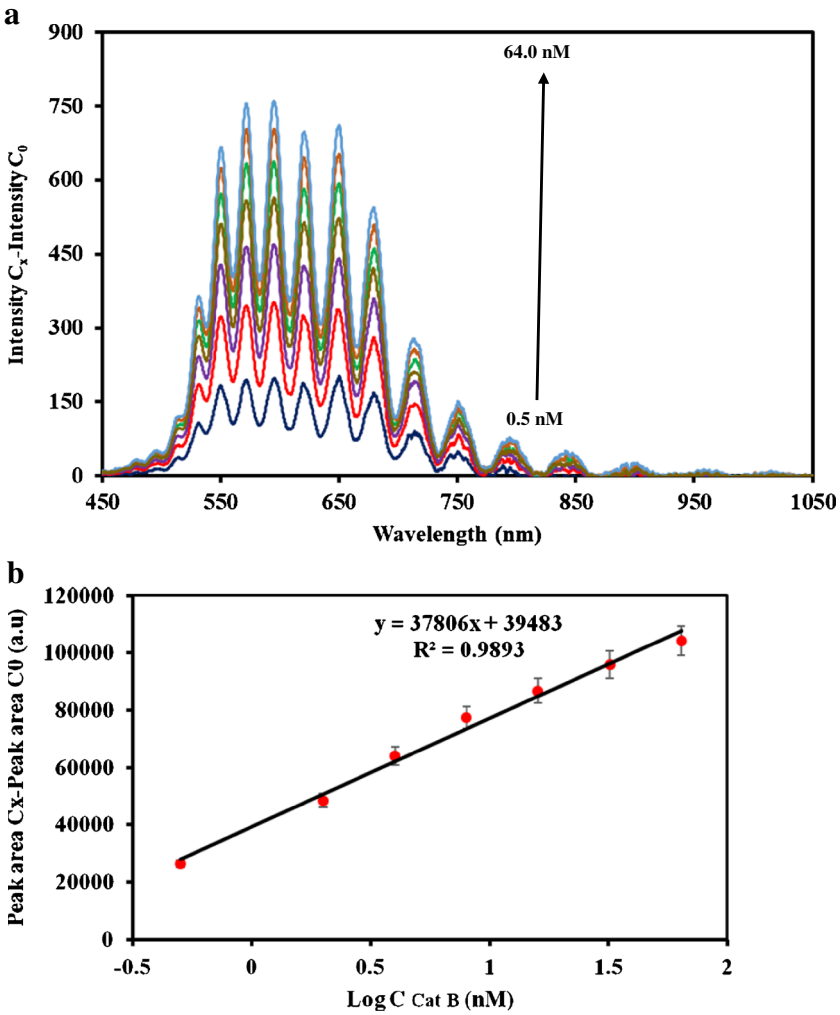

Fig. 6 **a** The difference between the Fabry-Perot fringe spectrum of NAA-Gla-HSA-TH in the absence and presence of different amounts of Cat B (0.5, 2.0, 4.0, 8.0, 16.0, 32.0, and 64.0 nM) at the optimum conditions acetate buffer (0.1 M, pH 5.0). **b** The calibration plot of the sensor toward Cat B. Each value is presented as mean ± SD, $n = 5$

The proteolysis kinetic of Cat B can be investigated with a modified Michaelis–Menten model (Eq. 1) [28].

$$\mathrm{E} + \mathrm{Ss} \underset{\mathrm{K-1}}{\overset{\mathrm{K1}}{\leftrightarrow}} \mathrm{ESs} \underset{\Rightarrow}{\overset{\mathrm{Kcat}}{}} \mathrm{E} + \mathrm{Ps} + \mathrm{P} \quad (1)$$

This heterogeneous enzymatic reaction rate (ds/dt) can be calculated according to Eq. (2)

$$-\frac{ds/dt}{S} = \frac{kcat}{Km}E0 \quad (2)$$

$-\frac{\mathrm{ds/dt}}{\mathrm{S}} = \frac{\mathrm{kcat}}{\mathrm{Km}}\mathrm{E0}$, where k_{cat} is the dissociation rate constant and K_M is the Michaelis–Menten constant, E_0 is the enzyme concentration, and S is the extracted proteolytic signal $\left(\frac{\text{signal t−signal b}}{\text{signal 0}}\right)$. In this equation, the $\frac{\mathrm{kcat}}{\mathrm{KM}}$ ratio that is referred to as the specificity constant has been commonly used for describing the efficiently Cat B. Therefore, the amount of the specificity constant is one of the analytical performances of the enzyme-based sensors that should be reported. The proteolysis kinetics represented by the extracted proteolysis signal $\left(\frac{\text{peak area t−peak area b}}{\text{peak area 0}}\right)$ versus the reaction time in the presence of 4 nM (a) and 11 nM (b) cathepsin B are shown in Fig. S2a. As can be seen, the extracted proteolysis signals decayed exponentially during the heterogeneous reactions. This plot can be used for the calculation of $\frac{\mathrm{kcat}}{\mathrm{KM}}$ ratio. For this purpose, the value of derivative of extracted proteolysis signal with respect to reaction time (ds/dt) (that has been obtained from Fig. S2A) is drawn versus S (Fig. S2b). The slope of the plot for 11 nM and 4 nM Cat B (E_0) were 1.4×10^{-3} $s^{-1}$and 0.533×10^{-3} s^{-1}, respectively. The average value of $\frac{\mathrm{kcat}}{\mathrm{KM}}$ was 12.7×10^{4} M^{-1} s^{-1}. This specificity constant is higher than in previous reports [2, 27, 29], suggesting that Cat B enzyme possesses higher catalytic efficiency in NAA-Gla-HSA-TH.

Table 1 Comparison of the analytical performance of the NAA-Gla-HSA-TH with other biosensors for the determination of Cat B

Sensor	Method	LDR/nM	LOD nM	K_{cat}/k_m ($\times 10^4$ M^{-1} s^{-1})	Ref
NEAs/VACNFs–$(CH_2)_4$–CO-Leu-Arg-Phe-Gly-NH–CH_2–Fc	ACV	15.5–62.1	15.5	9.2	[2]
NEAs/VACNFs-$(CH_2)_4$-CO-Pro-Leu-Arg-Phe-Gly-Ala-NH-CH_2-Fc	ACV	0.5–10.2	0.32	19	[3]
NEAs/VACNFs-$(CH_2)_4$-CO-Leu-Arg-Phe-Gly-NH-CH_2-Fc	ACV	Up to 30.7	–	4.3	[29]
NAA-Gla-HSA-TH	Optical	0.5–64	0.08	12.7	This work

NEAs Nanoelectrode arrays, *VACNFs* vertically aligned carbon nanofibers, *Fc* ferrocene, *ACV* alternating current voltammetry

The influence of interference, stability, and reproducibility of NAA-Gla-HSA-TH

The effect interfering with two common proteases (trypsin and urokinase) in a human serum sample was also studied to evaluate the selectivity of the sensor (Fig. S3a). As shown, the NAA-Gla-HSA-TH has a high selectivity to Cat B (32 nM) in the presence of 5 times excess of trypsin and urokinase. According to previous reports [30, 31], the enzyme activity of trypsin and urokinase is low in pH 5 solution that Cat B shows the maximum activity to cleave peptide. As can be seen from this figure, those enzymes did not have any interference effects on the signal of NAA-Gla-HSA-TH to Cat B. The enzymes' concentration was 20.0 times of Cat B (32 nM).

The effect of some small molecules such as urea, glucose, and dopamine on the response of NAA-Gla-HSA-TH was also evaluated (Fig. S3b). No sensible interference was also observed for 10^4-fold quantities of Cat B (32.0 nM). Therefore, the NAA-Gla-HSA-TH has high selectivity.

NAA-Gla-HSA-TH was applied for the determination of Cat B in normal human blood serum with the standard addition method to study its applicability in real sample analysis. Briefly, 0.1 mL of acetate buffer (0.1 M, pH 5.0) containing 80-nM Cat B was spiked into 9.9 mL of fresh human blood serum solution and shanked for 5 min. The solution was then injected into the analytical cell. Cat B concentration was determined to be 7.8 nM. The recovery of the analysis was 94%, regarding the amount obtained by the standard method [32]. NAA-Gla-HSA-TH was stored at 4 °C for 30 days to study the stability of the sensor. The intensity of the Fabry-Perot fringe spectrum decreased by 6.2%. This high stability of the NAA-Gla-HSA-TH can be related to the biocompatibility of NAA [33]. The reproducibility was also evaluated for determinations of 32 nM of Cat B with four different NAA-Gla-HSA-TH. The relative standard deviation (RSD) was 5.2% for Cat B.

Conclusions

A novel interferometric biosensor has been developed for the determination of Cat B based on the principle of digestion of the peptide by protease. NAA, HSA, and TH were used as nanoporous material, a peptide, and an optical probe, respectively, in this study. To immobilize TH to HSA, the carboxylic acid groups of HSA were activated by using EDC and NHS to interact with primary amines of TH. The immobilized TH adsorbed the transferred light to NAA, and therefore, the intensity of the reflected light to the CCD detector was low in the beginning. But in the presence of Cat B, HSA labeled with TH was digested to small peptide fragments, and then, the peptide fragment-TH washed away on NAA. Hence, the intensity of the reflected light from the NAA to the CCD detector increased. The enhanced intensity had a good linear relationship with the logarithm of the concentration of Cat B in the range of 0.5–64.0 nM. In Table 1, the analytical performances of the interferometric biosensor for the determination of Cat B are compared with NAA-Gla-HSA-TH. As can be observed, in most cases, the analytical performances of NAA-Gla-HSA-TH are better than the other sensors in the literature.

For the practical application of the current system, future efforts will focus on the fabrication of a portable sensor and the possibility of using it for the determination of the sample on the large scale.

Funding information This research was partially supported by a grant number RTI2018-094040-B-I00 from Spanish Ministerio de Ciencia, Innovación y Universidades (MICINN/FERDER), by the Agency for Management of University and Research Grants (AGAUR) with grant number 2017-SGR-1527, by the Catalan Institution for Research and Advanced Studies (ICREA) under the ICREA Academia Award and by the Martí-Franquès II postdoctoral program under Award Number 2017PMF-POST2-7. The project leading to these results has also received funding from the "la Caixa" Foundation under the agreement LCF/PR/PR17/11120023.

Compliance with ethical standards

Conflict of interest The authors declare that they have no competing interests

References

1. Shoji A, Suenaga Y, Hosaka A, Ishida Y, Yanagida A, Sugawara M (2017) Inhibitory assay for degradation of collagen IV by cathepsin

B with a surface plasmon resonance sensor. J Pharm Biomed Anal 145:79–83
2. Swisher LZ, Prior AM, Shishido S, Nguyen TA, Hua DH, Li J (2014) Quantitative electrochemical detection of cathepsin B activity in complex tissue lysates using enhanced AC voltammetry at carbon nanofiber nanoelectrode arrays. Biosens Bioelectron 56: 129–136
3. Song Y, Fan H, Anderson MJ, Wright JG, Hua DH, Koehne J, Meyyappan M, Li J (2019) Electrochemical activity assay for protease analysis using carbon nanofiber nanoelectrode arrays. Anal Chem 91:3971–3979
4. Wang Q, Yu L, Wong RCH, Lo P-C (2019) Construction of cathepsin B-responsive fluorescent probe and photosensitizer using a ferrocenyl boron dipyrromethene dark quencher. Eur J Med Chem 179:828–836
5. Shoji A, Kabeya M, Ishida Y, Yanagida A, Shibusawa Y, Sugawara M (2014) Evaluation of cathepsin B activity for degrading collagen IV using a surface plasmon resonance method and circular dichroism spectroscopy. J Pharm Biomed Anal 95:47–53
6. Amouzadeh Tabrizi M, Ferré-Borrull J, Marsal LF (2019) Highly sensitive aptasensor based on interferometric reflectance spectroscopy for the determination of amyloid β as an Alzheimer's disease biomarkers using nanoporous anodic alumina. Biosens Bioelectron 137:279–286
7. Rajeev G, Xifre-Perez E, Prieto Simon B, Cowin AJ, Marsal LF, Voelcker NH (2018) A label-free optical biosensor based on nanoporous anodic alumina for tumour necrosis factor-alpha detection in chronic wounds. Sensors Actuators B Chem 257:116–123
8. Pol L, Eckstein C, Acosta LK, Xifré-Pérez E, Ferré-Borrull J, Marsal LF (2019) Real-time monitoring of biotinylated molecules detection dynamics in nanoporous anodic alumina for bio-sensing. Nanomaterials 9:478
9. Macias G, Hernández-Eguía LP, Ferré-Borrull J, Pallares J, Marsal LF (2013) Gold-coated ordered nanoporous anodic alumina bilayers for future label-free interferometric biosensors. ACS Appl Mater Interfaces 5:8093–8098
10. Aguilar-Sierra SM, Ferré-Borrull J, Echeverría FE, Marsal LF (2019) Titanium dioxide-coated nanoporous anodic alumina optical properties. Appl Surf Sci 489:239–246
11. Lin VS-Y, Motesharei K, Dancil K-PS, Sailor MJ, Ghadiri MR (1997) A porous silicon-based optical interferometric biosensor. Science 278:840–843
12. Mun K-S, Alvarez SD, Choi W-Y, Sailor MJ (2010) A stable, label-free optical interferometric biosensor based on TiO2 nanotube arrays. ACS Nano 4:2070–2076
13. Eckstein C, Acosta LK, Pol L, Xifré-Pérez E, Pallares J, Ferré-Borrull J, Marsal LF (2018) Nanoporous anodic alumina surface modification by electrostatic, covalent, and immune complexation binding investigated by capillary filling. ACS Appl Mater Interfaces 10:10571–10579
14. Acosta LK, Bertó-Roselló F, Xifre-Perez E, Santos A, Ferré-Borrull J, Marsal LF (2019) Stacked nanoporous anodic alumina gradient-index filters with tunable multispectral photonic stopbands as sensing platforms. ACS Appl Mater Interfaces 11:3360–3371
15. Amouzadeh Tabrizi M, Ferré-Borrull J, Marsal LF (2020) Remote sensing of salmonella-specific DNA fragment by using nanoporous alumina modified with the single-strand DNA probe. Sensors Actuators B Chem 304:127302
16. Zhong Y-J, Shao L-H, Li Y (2012) Cathepsin B-cleavable doxorubicin prodrugs for targeted cancer therapy (review). Int J Oncol 42: 373–383
17. Göktürk S, Talman RY (2008) Effect of temperature on the binding and distribution characteristics of Thionine in sodium dodecyl sulfate micelles. J Solut Chem 37:1709–1723
18. Santos A, Balderrama VS, Alba M, Formentín P, Ferré-Borrull J, Pallarès J, Marsal LF (2012) Tunable Fabry-Pérot interferometer based on nanoporous anodic alumina for optical biosensing purposes. Nanoscale Res Lett 7:370–370
19. Santos A, Formentín P, Pallarès J, Ferré-Borrull J, Marsal LF (2011) Structural engineering of nanoporous anodic alumina funnels with high aspect ratio. J Electroanal Chem 655:73–78
20. Liu C, Shih K, Gao Y, Li F, Wei L (2012) Dechlorinating transformation of propachlor through nucleophilic substitution by dithionite on the surface of alumina. J Soils Sediments 12:724–733
21. Vasconcelos DCL, Nunes EHM, Vasconcelos WL (2012) AES and FTIR characterization of sol–gel alumina films. J Non-Cryst Solids 358:1374–1379
22. Pletincx S, Marcoen K, Trotochaud L, Fockaert L-L, Mol JMC, Head AR, Karslioğlu O, Bluhm H, Terryn H, Hauffman T (2017) Unravelling the chemical influence of water on the PMMA/aluminum oxide hybrid interface in situ. Sci Rep 7:13341–13351
23. Ayodhya D, Veerabhadram G (2016) Green synthesis, optical, structural, photocatalytic, fluorescence quenching and degradation studies of ZnS nanoparticles. J Fluoresc 26:2165–2175
24. Thenmozhi K, Sriman Narayanan S (2017) Carbon paste electrode with covalently immobilized thionine for electrochemical sensing of hydrogen peroxide. IOP Conference Series: Materials Science and Engineering 263:022031–022038
25. Ota C, Takano K (2016) Behavior of bovine serum albumin molecules in molecular crowding environments investigated by Raman spectroscopy. Langmuir 32:7372–7382
26. Yu M-E, Cheong B-S, Cho H-G (2017) SERS spectroscopy and DFT studies of thionine and its derivatives adsorbed on silver colloids: which N atom is used for coordination of a phenothiazine-based natural dye to electron-deficient metal surface? Bull Kor Chem Soc 38:928–934
27. Swisher LZ, Prior AM, Gunaratna MJ, Shishido S, Madiyar F, Nguyen TA, Hua DH, Li J (2015) Quantitative electrochemical detection of cathepsin B activity in breast cancer cell lysates using carbon nanofiber nanoelectrode arrays toward identification of cancer formation. Nanomedicine: Nanotechnology, Biol Med 11: 1695–1704
28. Gutiérrez OA, Chavez M, Lissi E (2004) A theoretical approach to some analytical properties of heterogeneous enzymatic assays. Anal Chem 76:2664–2668
29. Swisher LZ, Syed LU, Prior AM, Madiyar FR, Carlson KR, Nguyen TA, Hua DH, Li J (2013) Electrochemical protease biosensor based on enhanced AC voltammetry using carbon nanofiber nanoelectrode arrays. J Phys Chem C 117:4268–4277
30. Yabushita Y (1988) Studies on the properties of immobilized urokinase: effects of pH and temperature. Biotechnol Appl Biochem 10:294–300
31. Jung K-H, Choi Y-C, Chun J-Y, Min S-G, Hong G-P (2014) Effects of concentration and reaction time of trypsin, pepsin, and chymotrypsin on the hydrolysis efficiency of porcine placenta. Korean J Food Sci Anim Resour 34:151–157
32. Yhee JY, Kim SA, Koo H, Son S, Ryu JH, Youn I-C, Choi K, Kwon IC, Kim K (2012) Optical imaging of cancer-related proteases using near-infrared fluorescence matrix metalloproteinase-sensitive and cathepsin B-sensitive probes. Theranostics 2(2):179–189
33. La Flamme KE, Popat KC, Leoni L, Markiewicz E, La Tempa TJ, Roman BB, Grimes CA, Desai TA (2007) Biocompatibility of nanoporous alumina membranes for immunoisolation. Biomaterials 28:2638–2645